HHS Public Access

Author manuscript

Exp Eye Res. Author manuscript; available in PMC 2024 March 27.

Published in final edited form as:

Exp Eye Res. 2022 December ; 225: 109273. doi:10.1016/j.exer.2022.109273.

Microglia depletion exacerbates retinal ganglion cell loss in a mouse model of glaucoma

Zizhu Tan[(1),(2)], **Yinjie Guo**[(2),(3)], **Maleeka Shrestha**[(2)], **Daniel Sun**[(2)], **Meredith Gregory-Ksander**[(2)], **Tatjana C. Jakobs**[(2)]

[(1)]The First Affiliated Hospital of Xi'an Jiaotong University, 277 Yanta West Road, Xi'an, Shaanxi 710061, China

[(2)]Schepens Eye Research Institute/Massachusetts Eye and Ear, Harvard University School of Medicine, 20 Staniford Street, Boston, MA 02114

[(3)]The Second Xiangya Hospital of Central South University, 139 Middle Renmin Road, Changsha, Hunan 410011.

Abstract

To test whether depletion of microglia in the optic nerve head has a beneficial effect on retinal ganglion cell numbers and function, we depleted microglia by oral administration of the CSF1R antagonist PLX5622. Then, ocular hypertension was induced by unilateral injection of magnetic microbeads into the anterior chamber. Visual function was assessed with pattern electroretinography and measurement of the optomotor reflex. Retinal ganglion cell bodies and axons were counted and gene expression patterns in optic nerve head astrocytes were tested on freshly dissociated astrocytes. PLX5622 efficiently depleted microglia in the retina and the optic nerve head, but about 20% of microglia persisted in the myelinated optic nerve proper even after prolonged exposure to the drug. PLX5622 did not affect ganglion cell function by itself. Elevation of the IOP for four weeks led to the expected decrease in visual acuity and pattern ERG amplitude. Microglia ablation did not affect these parameters. Ganglion cell and axon numbers were counted histologically post mortem. Mice in the microglia depletion group showed a moderate but significantly greater loss of ganglion cells than the control group. At four weeks post microbead injection, gene expression patterns in optic nerve head astrocytes are consistent with an A2 (or neuroprotective) pattern. Microglia depletion blunted the up-regulation of A2 genes in astrocytes. In conclusion, microglia depletion is unlikely to protect retinal ganglion cells in early glaucoma.

Keywords

Glaucoma; microglia; CSF1R antagonist PLX5622; astrocytes; retinal ganglion cells; gene expression

1. Introduction

Astrocytes readily react to all kinds of CNS injuries such as trauma, hypoxia, inflammation, or neurodegenerative processes like glaucoma (Sofroniew, 2015; Sun and Jakobs, 2012). Astrocyte reactivity was historically described as process hypertrophy and up-regulation

of glial acidic fibrillary protein (GFAP). More recently, it has become clear that astrocyte reactivity is a complex program of changes in gene expression, cell morphology, and cell function that is dependent on the nature of the injury, the type of astrocyte, and the spatial and temporal distance of the astrocyte to the injury site (Oberheim et al., 2008; Wilhelmsson et al., 2006; Zamanian et al., 2012). Further complicating the matter, in different injury models, astrocyte reactivity can have beneficial or detrimental effects on the neurons they support. Astrocyte reactivity can be triggered by signals from neighboring cells, especially from microglia, and reciprocally influence microglia function, too (Matejuk and Ransohoff, 2020).

In some cases, such as neuroinflammation induced by LPS, microglia-derived TNF, C1q, and IL1 prompt astrocytes to assume a neurotoxic (or A1) phenotype, whereas other types of injury, e.g. arterial occlusion, lead to a more neuroprotective (or A2) phenotype (Liddelow et al., 2017; Zamanian et al., 2012). However, these should not be interpreted as fixed physiological types so that any astrocyte can only be the one or the other (Escartin et al., 2021). Rather, A1 and A2 phenotypes appear to be the ends of a spectrum of astrocyte reactivity that can change over time and possibly revert to the resting stage if the pathological stimulus is removed (Sun et al., 2013).

In glaucoma, changes in astrocyte and microglia morphology and gene expression profiles are observed even before retinal ganglion cell degeneration and visual function loss becomes obvious (Bosco et al., 2015; Bosco et al., 2011; Howell et al., 2011; Lye-Barthel et al., 2013; Tehrani et al., 2016; Tehrani et al., 2014; Wang et al., 2017). At least in early glaucoma, neuroprotective astrocyte functions dominate, and inhibiting astrocyte reactivity by conditional deletion of the transcription factor STAT3 leads to a worse outcome for ganglion cell survival and visual function (Sun et al., 2017). In the present study, we asked to what extent signaling from microglia influences astrocyte reactivity in the optic nerve head, whether astrocyte reactivity in early glaucoma can be classified as A1 or A2, and whether depleting microglia would protect ganglion cells and visual function. We used a modified microbead occlusion model of glaucoma (Chen et al., 2011; Sappington et al., 2010) with magnetic microbeads (Ito et al., 2016) to test the effect of microglia depletion with the CSF1R antagonist PLX5622 (Spangenberg et al., 2019) on visual function and ganglion cell and axon numbers. We also used single-cell RT-PCR of isolated astrocytes in the glial lamina region of the optic nerve to characterize the gene expression profile of reactive astrocytes.

2. Materials and Methods

Animals

All procedures conformed to the National Research Council's Guide for the Care and Use of Laboratory Animals and were approved by the Institutional Animal Care and Use Committee of the Schepens Eye Research Institute. Equal numbers of male and female C57bl/6 mice (Jackson Laboratory, stock number 000664) aged 6 weeks at the beginning of the experiment were group-housed in a 12-hour light/dark environment and received food and water ad libitum. Animal numbers for all experiments are summarized in Supplementary Table 1. In addition, we used heterozygous B6.129P-Cx3cr1^{tm1Litt}/J (B6.Cx3cr1-GFP,

Jackson Laboratory, stock number 005582) mice that express a green fluorescent protein (GFP) in microglia and macrophages under the control of the Cx3cr1 promoter (Xavier et al., 2015).

Microglia depletion

Microglia were depleted by administering PLX5622, an inhibitor of the colony-stimulating factor 1 receptor, in the chow (Elmore et al., 2014). PLX5622 was purchased from Chemgood LLC and formulated in irradiated AIN-76A standard rodent chow by Research Diets, Inc. at 1200 ppm, equivalent to 0.2 mg/kg/day/mouse. Mice were placed on the PLX5622 diet for 3 weeks before injection of microbeads. Control animals received the standard rodent chow without the inhibitor. Microglia depletion was monitored by including a group of 6 sentinel heterozygous B6.Cx3cr1-GFP mice. Normal (undepleted) microglia were counted from 7 B6.Cx3cr1-GFP mice that had received the control diet.

Microbead occlusion model and IOP measurements

B6 mice were anesthetized with an intraperitoneal injection of a combination solution of 100 mg/ mL ketamine and 20 mg/mL xylazine. After administering 1% tropicamide (Bausch and Lomb, Tampa, FL) and 0.5% proparacaine hydrochloride (Akorn, Lake Forest, IL) to the eye, 2.0 μl of a suspension of magnetic microbeads (4.5 μm diameter, 1.6×10^6 beads/μl in PBS) were injected into the anterior chamber of the right eyes using a microsyringe pump and a microneedle with a facetted bevel (Ito et al., 2016). A hand-held magnet was used to attract the magnetic microbeads to the iridocorneal angle to prevent the drainage of aqueous humor from the anterior chamber. The left eye was left untreated. IOP elevation in one eye can lead to microglia activation in the contralateral eye (Tribble et al., 2021). Therefore, we used an independent saline-injected group of 10 mice as controls. In this group, 2.0 μl of 0.1 M phosphate buffer solution (PBS) was injected into the anterior chamber of the right eye. IOP was measured with a rebound tonometer (TonoLab; ICare, Raleigh, NC) under light isoflurane anesthesia (1.5% delivered via a nosecone). Five readings were taken from each eye and averaged. All measurements were taken at the same time of the day (10 am) to avoid circadian variation. A baseline IOP reading was taken before the eyes were injected with magnetic microbeads or saline. After the ocular injection procedure, IOP measurements were taken every three days for a total of 4 weeks.

Optomotor reflex and pattern electroretinogram

The visual acuity was measured by an optomotor reflex-based spatial frequency threshold test (Gao and Jakobs, 2016; Prusky et al., 2004). Awake mice were placed on a platform (2-inch diameter) located in the center of four computer monitors arranged in a square. Each monitor showed a moving vertical black and white sinusoidal grating pattern. The clockwise and counterclockwise rotation directions of the pattern provide independent temporal-to-nasal stimulation of the left and right eyes, respectively (Douglas et al., 2005). The rotation speed (12 /sec) and contrast (100%) remained constant. The distance between the bars of the pattern varied between 350 and 11 mm, corresponding to 0.02 to 0.46 cycles/degree. The highest spatial frequency that elicited tracking behavior was recorded as the visual acuity. Experimenters were blinded to the treatment and IOP history of the mice.

Pattern electroretinogram (PERG) recordings were performed on a Celeris small animal testing system (Diagnosys LLC, Lowell, MA). After dark adaptation (>14 hours), animals were anesthetized with ketamine and xylazine, followed by pupil dilation and corneal anesthesia as described above. Body temperature was maintained at 37 °C using the built-in warming platform of the recording setup. The reversing checkerboard pattern was provided by a specialized stimulus/recording electrode that directly contacts the cornea; an electrode on the other eye served as a reference. Artificial tears (0.3% Hypromellose, Genteal; Alcon, TX) were used to improve contact between the cornea and the recording electrodes. Both eyes were measured consecutively in the same session. PERG amplitude is reported as the difference between the positive peak (P1) and N2 (negative) in μV.

Tissue preparation

After euthanasia, the skull was opened, and the brain was removed to expose the optic nerve and optic chiasm to obtain an eye and optic nerve without causing structural damage (Sun et al., 2010). The head was fixed in 4% paraformaldehyde for 2 hours at room temperature and then rinsed in PBS. Thereafter, eyeballs and optic nerves were dissected free of the surrounding tissue, including the dura mater around the optic nerve. The cornea was cut along the limbus to remove the lens and vitreous. The optic nerve was gently separated from the retina, and the remaining sclera was removed. For ganglion cell counting, retinas were whole-mounted on AA nitrocellulose filter (MF-Millipore, Billerica, MA). For optic nerve head immunohistochemistry, the optic nerve heads were cryoprotected in 30% sucrose overnight, embedded in OCT compound (Ted Pella, Redding, CA), and sectioned at a thickness of 14 μm.

PPD staining and axon counting

Optic nerves proper were post-fixed in half-strength Karnovski's fixative (2% formaldehyde/ 2.5% glutaraldehyde in 0.1 mol/L sodium cacodylate buffer; Electron Microscopy Sciences, Hatfield, PA) overnight at 4 °C, embedded in tEpon-812 (Tousimis, Rockville, MD) and thin sectioned (0.5 μm) before staining with 2% paraphenylenediamine (PPD, MP Biomedicals, Solon, OH) in aqueous solution (Mukai et al., 2019). Nerves stained with PPD were imaged on a Nikon microscope (Eclipse E800, Nikon, Japan) at 40× magnification. Images of 5 non-overlapping rectangular regions were taken that nearly covered the entire area of each optic nerve cross-section, and 50 μm x 50 μm square regions were used to count axons. The average axon count in 5 images was used to calculate the axon density (axons/mm^2). The cross-sectional area of the optic nerve was measured in ImageJ (version 1.48v, NIH, Bethesda, MD; http://imagej.nih.gov/ij) and used to calculate total axon numbers.

Immunohistochemistry

For ganglion cell counting, retinas were incubated with primary antibodies at 4°C with shaking for 3 days, then washed, incubated with secondary antibodies overnight, and counterstained with DAPI (Life Technologies, Grand Island, NY). Primary antibodies were mouse anti-Brn3a (dilution 1:200; EMD Millipore, Billerica, MA), anti-TMEM119 (dilution 1:200, Abcam, Waltham, MA), anti-CSF1R (dilution 1:100, Abcam), and rabbit anti-NF-h (dilution 1:600; Novus biologicals, Centennial, CO). All FITC- or tetramethylrhodamine-conjugated secondary antibodies were obtained from Jackson Immunoresearch Laboratories

(West Grove, PA). Finally, retinas were mounted with Vectashield (Vector, Burlingame, CA). Sections of optic nerve heads were stained on-slide with primary antibodies to chicken anti-GFAP (dilution 1:2000; Abcam, Cambridge, MA) for astrocytes or rabbit anti-NF-h for ganglion cell axons. Sections were incubated with secondary antibodies and counterstained with DAPI before mounting with Vectashield.

Microscopy and quantification

Images were acquired on a Leica TCS SP8 confocal microscope (Leica Microsystems, Wetzlar, Germany). For ganglion cell counting, the retina was divided into four quadrants, and two areas equidistant to the optic nerve head and the rim of the retina were imaged per quadrant resulting in a total of 8 images (each area 290.91 μm x 290.91 μm). For ganglion cell counting, Z-stacks (step size, 0.5 microns) through the ganglion cell layer were maximum-intensity projected in ImageJ. We used Photoshop CS6 (Adobe, San Jose, CA) to adjust the brightness and contrast of the final image; no other digital image processing was performed.

Optic nerve dissociation and single-cell RT-PCR

For single astrocyte dissociation, fresh unfixed optic nerve heads were first treated with Hank's balanced salt solution (HBSS) containing papain (35 mg/mL, Worthington Biochemical, Lakewood, NJ) and L-cysteine (10 mg/ml, Gibco BRL, NY), and then washed with HBSS containing 10% horse serum and 60 U/ml DNase. Then the cell suspension was triturated using a series of heat-polished Pasteur pipettes and resuspended in cold PBS. Individual astrocytes were identified on a Zeiss Axiovert200 equipped with micromanipulators and aspirated into glass micropipets (Choi et al., 2015). Cells were washed in fresh PBS and transferred into thin-wall PCR tubes under optical control. From each sample, 12 individual cells were pooled. Total RNA was extracted from the astrocytes using the RNeasy Plus Micro Kit (Qiagen, Germantown, MD), and cDNA synthesis was performed using the NEB Next Single Cell/Low Input cDNA Synthesis & Amplification Module (New England Biolabs, Ipswich, MA) according to supplier protocols. The amplified cDNAs were diluted at 1:5 as a template for quantitative real-time PCR (qRT-PCR) using SYBR Green PCR Master Mix (Applied Biosystems, Foster City, CA). Primers were designed to span intron/exon boundaries using NCBI primer BLAST software (http://www.ncbi.nlm.nih.gov/tools/primer-blast/) and were purchased from Eurofins MWG Operon (Louisville, KY). Primer sequences are given in Supplementary Table 2. Glyceraldehyde phosphate dehydrogenase (GAPDH) was used as a housekeeping gene control for calculations of the ΔCt values because GAPDH expression level in the optic nerve is relatively stable in experimental glaucoma (Johnson et al., 2011). A gene was considered differentially expressed if the expression level at any of the time points (7d, 14d, 21d, or 28d) was significantly different from baseline levels by ANOVA with the p value adjusted for multiple comparisons.

Data Analysis

Ganglion and axon cell counts were imported from ImageJ to Matlab, and groups were compared by ANOVA followed by the Tukey-Cramer post hoc test. All data are presented as averages ± SD. All data from individual mice (IOP, visual acuity, pERG amplitude,

retinal ganglion cell counts, axon counts, and astrocyte process thickness) are reported in Supplementary Table 3.

3. Results

3.1. Microglia depletion

Seven B6.Cx3crGFP mice were used to determine baseline microglia densities in the retina and optic nerve. Sentinel B6.Cx3crGFP mice were administered PLX5622 to assess the extent of microglia depletion. After 3 and 7 weeks on the diet, 3 sentinels each were euthanized, and retinas and optic nerves were imaged. In the optic nerve head, almost all GFP^+ cells were eliminated after 3 weeks on the PLX5622 diet; however, there was a small number of persistent GFP^+ cells in the ONH (Figure 1A). In the retina and the optic nerve proper, more GFP^+ cells persisted even after 7 weeks on the PLX6522 diet (Figure 1B). Expression of GFP under the control of the Cx3cr1 promoter does not distinguish between microglia and macrophages, both of which express the marker. We, therefore, counterstained the tissue with an antibody to TMEM119, one of the molecules that have been described as specific to microglia (Bennett et al., 2016). All GFP^+ cells in the retina and optic nerve were also positive for TMEM119 labeling and likely are microglia (Figure 2). We also counterstained the cells with an antibody against CSF1R (CD115), the target of PLX5622. Though all GFP^+ cells were also labeled with the CSF1R antibody, there were differences in the staining intensity, suggesting that some microglia either express lower levels of the receptor or down-regulate it in response to PLX5622, which may explain their resistance to the drug. As we were most interested in interactions between microglia and astrocytes in the optic nerve head, and administration of PLX5622 had little additional effect on the optic nerve beyond 3 weeks, we decided to use this time point to start inducing elevated IOP.

3.2. Assessment of visual function in microglia-depleted and control animals

C57bl/6 mice were given a baseline eye exam consisting of IOP measurement, pattern ERG (pERG), and assessment of the visual acuity by observing the oculomotor reflex. The mice were then divided into 2 groups with equal numbers of male and female mice; 32 of them received mouse chow containing PLX5622, and 28 received the control diet without the drug for 3 weeks (Figure 3 shows a schematic of the experimental groups, Supplementary Table 1 shows numbers of mice in each experimental group). At this point, pERG and visual acuity were tested again. Microglia depletion alone did not affect visual function. Then, both groups were divided further into 2 groups, one of which received injections of magnetic microbeads into the anterior chamber, and the other group was injected with sterile saline solution alone. The IOP was measured twice weekly in all groups until the end of the experimental period (4 weeks). To estimate the severity of the IOP insult in all groups, we determined the mean IOP and the cIOP (cumulative IOP) as the area under the curve of the IOP versus time (Supplementary Figure 1 and Figure 4A-B). In one case, the IOP did not rise at all. This animal was excluded from all further analyses. Microbead injection led to a significant increase in mean IOP and cIOP, but there was no difference between the control diet and the PLX5622 groups (cIOPs were 393 ± 9.75 vs. 381 ± 14.3 mmHgdays in the saline-injected groups and 498.91 ± 67.03 and 516.83 ± 62.17 mmHgdays in the microbead injected groups, $p=0.57$ for the comparison of control and depletion diet). This indicates

that both groups had experienced a similar IOP insult. At 4 weeks after microbead or saline injection, we tested pERG and visual acuity again. Elevated IOP led to the expected decrease in pERG amplitude compared to the saline-injected control group (pERG amplitude loss was 6.18 ± 5.1 μV in the group on the control diet and 8.66 ± 5.3 μV on the depletion diet), but there was no significant difference between the two groups (p=0.34, Figure 4C). Visual acuity decreased from 0.42 cycles/degree in saline-injected eyes to 0.29 ± 0.052 and 0.27 ± 0.043 cycles/degree in the microbead injected animals on control and depletion diet, respectively (p=0.38, Figure 4D).

3.4. Retinal ganglion cell and axon loss

The retinas from all mice were isolated and stained for the ganglion cell marker Brn3a to quantify ganglion cell loss (Figure 5A). The average RGC density in mid-periphery was 3568.46 ± 171 in the control eyes (saline-injected, normal diet, n=4). Retinas from microglia-depleted eyes with saline injection had 3700.28 ± 266.11 ganglion cells/mm^2 (n=6), indicating that microglia depletion by itself does not change retinal ganglion cell counts. In microglia-depleted (n=9) and control groups (n=8), IOP elevation led to a significant reduction of ganglion cell bodies, which is expected for this model. However, microglia-depleted mice lost more ganglion cells after microbead injection than did the non-depleted group (2802.24 ± 154.01 cells/mm^2 versus 3049.86 ± 186.75 cells/mm^2, or a 25.9% loss versus a 17.3% loss, respectively, p=0.009, Figure 5C). Ganglion cell axons were stained in the myelinated part of the optic nerve proper after PPD staining. In the control group (non-depleted, saline injection), 48932.77 ± 4517.37 axons were counted , which is well inside the normal range for C56bl/6 mice (Zhu et al., 2018). In the microbead group, axon counts were 38957.69 ± 4042.41. For the microglia depletion groups, axons counts were 47656.06 ± 6054.71 and 33757.35 ± 2951.06 for the saline-injected and the microbead-injected eyes, respectively. Comparing the non-depleted with the microglia-depleted high IOP groups, this was significantly different (p=0.012, Figure 5D).

3.5. Reactive astrocyte morphology

After one month of IOP elevation, optic nerve astrocytes show morphological signs of reactivity, such as hypertrophy of their processes and a loss of the typical “honeycomb” organization of the glial lamina that is characterized by the arrangement of astrocytes into glial tubes through which the ganglion cell axon bundles pass (Wang et al., 2017). We tested whether these morphological changes would be affected by microglia depletion (Figure 6A-D). In saline-injected control eyes, the average thickness of astrocyte processes was 1.38 ± 0.17 μm in microglia-depleted (n=4) nerves versus 1.29 ± 0.13 μm in nerves from the control group (n=4, n.s. with p=0.42). Glial tubes were obvious in both groups. Microbead injection led to an expected process hypertrophy and loss of glial tubes; however, there was no difference between the depleted (n=7) and control (n=7) conditions (Figure 6C-D, 1.94 ± 0.06 μm and 1.81 ± 0.11 μm, respectively, p=0.13). Quantification of astrocyte process thickness is shown in Figure 6E.

3.6. Profiling of reactive astrocytes

We then tested whether microglia depletion affected astrocytic gene expression, in particular on the neurotoxic (A1) versus the neuroprotective (A2) pattern of astrocyte reactivity

markers. Mice were treated with PLX5622 or a control diet for 3 weeks as described above and divided into baseline, microbead- and saline-injected groups (Figure 3, Supplementary Table 1). At 7, 14, 21, and 28 days after microbead or saline injection, mice were sacrificed. Since the optic nerve head contains microglia and endothelial cells in addition to astrocytes, the optic nerve heads were dissociated into single cells. From each nerve head, 12 astrocytes were identified under microscopic control and pooled for RNA extraction and RT-PCR detection of A1 and A2 genes. With one exception (Amigo2), all of the marker genes were detectable in optic nerve astrocytes; however, not all of them changed with IOP elevation. In particular, in the A1 group, only 4 genes were up-regulated at any time point after IOP elevation (Figure 7). Eight of the A2-specific genes were significantly up-regulated at least at one time point after IOP elevation. Treatment with PLX5622 blunted the up-regulation of A2 genes, particularly for the markers S100a10 and Slc10a6. Emp1 showed the opposite behavior, and Tgm1 was unaffected by microglia ablation (Figure 7).

4. Discussion

In animal models of glaucoma, changes to morphology and gene expression of microglial cells are amongst the earliest signs of pathology that precede ganglion cell degeneration and death (Bosco et al., 2015; Bosco et al., 2011; Tribble et al., 2020; Yuan and Neufeld, 2001). Micro- and macroglia communicate with each other through a variety of secretory factors (such as IFNγ, TNFα, or interleukins 1 and 6) that may influence whether astrocytes take on a neuroprotective or neurotoxic role (Guttenplan et al., 2020; Guttenplan et al., 2021; Liddelow et al., 2017; Zhao et al., 2021). In analogy to microglia, which are often described as inflammation-promoting "M1" microglia and anti-inflammatory "M2" microglia, astrocytes have been divided into neurotoxic “A1” and neuroprotective “A2” astrocytes. Both groups are characterized by the up-regulation of small groups of marker genes (Liddelow et al., 2017). However, as with “M1” and “M2” microglia, large-scale gene expression surveys in different disease models have complicated the picture (Escartin et al., 2021; Ransohoff, 2016). Originally, A1 and A2 gene up-regulation was described in LPS-induced neuroinflammation, and middle cerebral artery occlusion, respectively (Zamanian et al., 2012); but the neuroprotective or detrimental effects of astrocyte reactivity are highly context-dependent, and in several other models, no clear patterns of A1 or A2 genes were observed (Das et al., 2020). Optic nerve astrocytes in early glaucoma are amongst those that do show a relatively clear A2 pattern – in our study, 8 out of 12 genes in the A2 group were up-regulated after an increase of IOP (in contrast to 4 out of 12 A1 genes), suggesting a predominantly neuroprotective role of astrocytes in this context. This is consistent with evidence showing that interfering with astrocyte reactivity (by tissue-specific deletion of the Stat3 gene) leads to a worse outcome for retinal ganglion cell survival and visual function in mouse models of glaucoma (Sun et al., 2017). Microglia ablation led to a reduction of A2 gene up-regulation (with the exceptions of Emp1 and Tgm1), whereas the effect on A1 genes was the opposite; most A1 genes were more strongly up-regulated in the microglia depleted group (except for H2-D1).

These findings are in contrast to reports from the literature that suggest a more negative role for activated microglia in early glaucoma. Guttenplan and colleagues found that in IL1a/TNFα/C1qa triple knock-out mice retinal ganglion cells are protected after optic nerve

crush injury and in a model of glaucoma (Guttenplan et al., 2020). As IL1a, C1q, and TNF are inductors of neurotoxic astrocytes (Liddelow et al., 2017) this would suggest that microglia instruct astrocytes to assume a neurotoxic phenotype in these models. The main difference of this report to our present study is that we did not delete specific genes that are known inductors of A1 astrocytes, but eliminated microglia completely. This would certainly lower the total amounts of IL1a, C1q, or TNF that is secreted by microglia, but it would also reduce secretion of factors that induce neuroprotective astrocytes and, of course, eliminate the physiological functions of the microglia themselves, such as debris clearance. As reported previously, eliminating microglia with PLX5622 before middle cerebral artery occlusion resulted in a worse functional outcome and significantly increased infarct site (Szalay et al., 2016), suggesting that the effect is not peculiar to the optic nerve.

A second approach using minocycline to inhibit microglia activation proved to be protective in the DBA/2J model of glaucoma (Bosco et al., 2008), again suggesting a more destructive role of microglia in retinal ganglion cell survival. However, while minocycline is known to reduce microglia activation and to be neuroprotective in several injury models (Grotegut et al., 2020; Ozaki et al., 2022; Tikka et al., 2001; Yrjanheikki et al., 1999), its pleiotropic effects complicate the analysis. Minocycline also affects other immune cells, such as macrophages and T-cells (Dunston et al., 2011; Szeto et al., 2011), both of which may be involved in glaucoma (Chen et al., 2018; Howell et al., 2012). In addition, minocycline has been shown to enhance the survival of neurons in cell culture directly, even in the absence of microglia (Huang et al., 2010; Schildknecht et al., 2011).

Taken together, our experiments show that specific ablation of microglia does not prevent retinal ganglion cell loss in the microbead model of ocular hypertension. Rather, we observed a significantly greater loss of ganglion cells and axons in the PLX5622 group. The effect was relatively modest (25.9% vs. 17.3%). This may be because whereas the retina and the unmyelinated portion of the optic nerve were cleared of almost all detectable microglia, about 20% of the $TMEM119^{+}$ microglial cells persisted in the optic nerve proper even after prolonged exposure to the drug, possibly limiting the effect. However, even the incomplete ablation of optic nerve microglia had a measurable detrimental effect on ganglion cell survival. It is, therefore, unlikely that complete depletion of retinal and optic nerve microglia would prevent glaucomatous ganglion cell loss.

Supplementary Material

Refer to Web version on PubMed Central for supplementary material.

Acknowledgments

This work was supported by grants R01EY019703, R21EY030276, the NIH Core Grant for Vision Research P30EY003790, and a grant from the Massachusetts Lions Eye Research Fund. The authors have no conflicts of interest to disclose.

6. References

Bennett ML, Bennett FC, Liddelow SA, Ajami B, Zamanian JL, Fernhoff NB, Mulinyawe SB, Bohlen CJ, Adil A, Tucker A, Weissman IL, Chang EF, Li G, Grant GA, Hayden Gephart MG, and Barres

BA. 2016. New tools for studying microglia in the mouse and human CNS. Proc Natl Acad Sci U S A. 113:E1738–1746. [PubMed: 26884166]

Bosco A, Inman DM, Steele MR, Wu G, Soto I, Marsh-Armstrong N, Hubbard WC, Calkins DJ, Horner PJ, and Vetter ML. 2008. Reduced retina microglial activation and improved optic nerve integrity with minocycline treatment in the DBA/2J mouse model of glaucoma. Invest Ophthalmol Vis Sci. 49:1437–1446. [PubMed: 18385061]

Bosco A, Romero CO, Breen KT, Chagovetz AA, Steele MR, Ambati BK, and Vetter ML. 2015. Neurodegeneration severity can be predicted from early microglia alterations monitored in vivo in a mouse model of chronic glaucoma. Dis Model Mech. 8:443–455. [PubMed: 25755083]

Bosco A, Steele MR, and Vetter ML. 2011. Early microglia activation in a mouse model of chronic glaucoma. J Comp Neurol. 519:599–620. [PubMed: 21246546]

Chen H, Cho KS, Vu THK, Shen CH, Kaur M, Chen G, Mathew R, McHam ML, Fazelat A, Lashkari K, Au NPB, Tse JKY, Li Y, Yu H, Yang L, Stein-Streilein J, Ma CHE, Woolf CJ, Whary MT, Jager MJ, Fox JG, Chen J, and Chen DF. 2018. Commensal microflora-induced T cell responses mediate progressive neurodegeneration in glaucoma. Nat Commun. 9:3209. [PubMed: 30097565]

Chen H, Wei X, Cho KS, Chen G, Sappington R, Calkins DJ, and Chen DF. 2011. Optic neuropathy due to microbead-induced elevated intraocular pressure in the mouse. Invest Ophthalmol Vis Sci. 52:36–44. [PubMed: 20702815]

Choi HJ, Sun D, and Jakobs TC. 2015. Isolation of intact astrocytes from the optic nerve head of adult mice. Exp Eye Res. 137:103–110. [PubMed: 26093274]

Das S, Li Z, Noori A, Hyman BT, and Serrano-Pozo A. 2020. Meta-analysis of mouse transcriptomic studies supports a context-dependent astrocyte reaction in acute CNS injury versus neurodegeneration. J Neuroinflammation. 17:227. [PubMed: 32736565]

Douglas RM, Alam NM, Silver BD, McGill TJ, Tschetter WW, and Prusky GT. 2005. Independent visual threshold measurements in the two eyes of freely moving rats and mice using a virtual-reality optokinetic system. Vis Neurosci. 22:677–684. [PubMed: 16332278]

Dunston CR, Griffiths HR, Lambert PA, Staddon S, and Vernallis AB. 2011. Proteomic analysis of the anti-inflammatory action of minocycline. Proteomics. 11:42–51. [PubMed: 21182193]

Elmore MR, Najafi AR, Koike MA, Dagher NN, Spangenberg EE, Rice RA, Kitazawa M, Matusow B, Nguyen H, West BL, and Green KN. 2014. Colony-stimulating factor 1 receptor signaling is necessary for microglia viability, unmasking a microglia progenitor cell in the adult brain. Neuron. 82:380–397. [PubMed: 24742461]

Escartin C, Galea E, Lakatos A, O'Callaghan JP, Petzold GC, Serrano-Pozo A, Steinhauser C, Volterra A, Carmignoto G, Agarwal A, Allen NJ, Araque A, Barbeito L, Barzilai A, Bergles DE, Bonvento G, Butt AM, Chen WT, Cohen-Salmon M, Cunningham C, Deneen B, De Strooper B, Diaz-Castro B, Farina C, Freeman M, Gallo V, Goldman JE, Goldman SA, Gotz M, Gutierrez A, Haydon PG, Heiland DH, Hol EM, Holt MG, Iino M, Kastanenka KV, Kettenmann H, Khakh BS, Koizumi S, Lee CJ, Liddelow SA, MacVicar BA, Magistretti P, Messing A, Mishra A, Molofsky AV, Murai KK, Norris CM, Okada S, Oliet SHR, Oliveira JF, Panatier A, Parpura V, Pekna M, Pekny M, Pellerin L, Perea G, Perez-Nievas BG, Pfrieger FW, Poskanzer KE, Quintana FJ, Ransohoff RM, Riquelme-Perez M, Robel S, Rose CR, Rothstein JD, Rouach N, Rowitch DH, Semyanov A, Sirko S, Sontheimer H, Swanson RA, Vitorica J, Wanner IB, Wood LB, Wu J, Zheng B, Zimmer ER, Zorec R, Sofroniew MV, and Verkhratsky A. 2021. Reactive astrocyte nomenclature, definitions, and future directions. Nat Neurosci. 24:312–325. [PubMed: 33589835]

Gao S, and Jakobs TC. 2016. Mice Homozygous for a Deletion in the Glaucoma Susceptibility Locus INK4 Show Increased Vulnerability of Retinal Ganglion Cells to Elevated Intraocular Pressure. Am J Pathol. 186:985–1005. [PubMed: 26883755]

Grotegut P, Perumal N, Kuehn S, Smit A, Dick HB, Grus FH, and Joachim SC. 2020. Minocycline reduces inflammatory response and cell death in a S100B retina degeneration model. J Neuroinflammation. 17:375. [PubMed: 33317557]

Guttenplan KA, Stafford BK, El-Danaf RN, Adler DI, Munch AE, Weigel MK, Huberman AD, and Liddelow SA. 2020. Neurotoxic Reactive Astrocytes Drive Neuronal Death after Retinal Injury. Cell Rep. 31:107776. [PubMed: 32579912]

Guttenplan KA, Weigel MK, Prakash P, Wijewardhane PR, Hasel P, Rufen-Blanchette U, Munch AE, Blum JA, Fine J, Neal MC, Bruce KD, Gitler AD, Chopra G, Liddelow SA, and Barres BA.

2021. Neurotoxic reactive astrocytes induce cell death via saturated lipids. Nature. 599:102–107. [PubMed: 34616039]

Howell GR, Macalinao DG, Sousa GL, Walden M, Soto I, Kneeland SC, Barbay JM, King BL, Marchant JK, Hibbs M, Stevens B, Barres BA, Clark AF, Libby RT, and John SW. 2011. Molecular clustering identifies complement and endothelin induction as early events in a mouse model of glaucoma. J Clin Invest. 121:1429–1444. [PubMed: 21383504]

Howell GR, Soto I, Zhu X, Ryan M, Macalinao DG, Sousa GL, Caddle LB, MacNicoll KH, Barbay JM, Porciatti V, Anderson MG, Smith RS, Clark AF, Libby RT, and John SW. 2012. Radiation treatment inhibits monocyte entry into the optic nerve head and prevents neuronal damage in a mouse model of glaucoma. J Clin Invest. 122:1246–1261. [PubMed: 22426214]

Huang WC, Qiao Y, Xu L, Kacimi R, Sun X, Giffard RG, and Yenari MA. 2010. Direct protection of cultured neurons from ischemia-like injury by minocycline. Anat Cell Biol. 43:325–331. [PubMed: 21267407]

Ito YA, Belforte N, Cueva Vargas JL, and Di Polo A. 2016. A Magnetic Microbead Occlusion Model to Induce Ocular Hypertension-Dependent Glaucoma in Mice. J Vis Exp:e53731. [PubMed: 27077732]

Johnson EC, Doser TA, Cepurna WO, Dyck JA, Jia L, Guo Y, Lambert WS, and Morrison JC. 2011. Cell proliferation and interleukin-6-type cytokine signaling are implicated by gene expression responses in early optic nerve head injury in rat glaucoma. Invest Ophthalmol Vis Sci. 52:504–518. [PubMed: 20847120]

Liddelow SA, Guttenplan KA, Clarke LE, Bennett FC, Bohlen CJ, Schirmer L, Bennett ML, Munch AE, Chung WS, Peterson TC, Wilton DK, Frouin A, Napier BA, Panicker N, Kumar M, Buckwalter MS, Rowitch DH, Dawson VL, Dawson TM, Stevens B, and Barres BA. 2017. Neurotoxic reactive astrocytes are induced by activated microglia. Nature. 541:481–487. [PubMed: 28099414]

Lye-Barthel M, Sun D, and Jakobs TC. 2013. Morphology of astrocytes in a glaucomatous optic nerve. Invest Ophthalmol Vis Sci. 54:909–917. [PubMed: 23322566]

Matejuk A, and Ransohoff RM. 2020. Crosstalk Between Astrocytes and Microglia: An Overview. Front Immunol. 11:1416. [PubMed: 32765501]

Mukai R, Park DH, Okunuki Y, Hasegawa E, Klokman G, Kim CB, Krishnan A, Gregory-Ksander M, Husain D, Miller JW, and Connor KM. 2019. Mouse model of ocular hypertension with retinal ganglion cell degeneration. PLoS One. 14:e0208713. [PubMed: 30640920]

Oberheim NA, Tian GF, Han X, Peng W, Takano T, Ransom B, and Nedergaard M. 2008. Loss of astrocytic domain organization in the epileptic brain. J Neurosci. 28:3264–3276. [PubMed: 18367594]

Ozaki E, Delaney C, Campbell M, and Doyle SL. 2022. Minocycline suppresses disease-associated microglia (DAM) in a model of photoreceptor cell degeneration. Exp Eye Res. 217:108953. [PubMed: 35090890]

Prusky GT, Alam NM, Beekman S, and Douglas RM. 2004. Rapid quantification of adult and developing mouse spatial vision using a virtual optomotor system. Invest Ophthalmol Vis Sci. 45:4611–4616. [PubMed: 15557474]

Ransohoff RM 2016. A polarizing question: do M1 and M2 microglia exist? Nat Neurosci. 19:987–991. [PubMed: 27459405]

Sappington RM, Carlson BJ, Crish SD, and Calkins DJ. 2010. The microbead occlusion model: a paradigm for induced ocular hypertension in rats and mice. Invest Ophthalmol Vis Sci. 51:207–216. [PubMed: 19850836]

Schildknecht S, Pape R, Muller N, Robotta M, Marquardt A, Burkle A, Drescher M, and Leist M. 2011. Neuroprotection by minocycline caused by direct and specific scavenging of peroxynitrite. J Biol Chem. 286:4991–5002. [PubMed: 21081502]

Sofroniew MV 2015. Astrogliosis. Cold Spring Harb Perspect Biol. 7:a020420.

Spangenberg E, Severson PL, Hohsfield LA, Crapser J, Zhang J, Burton EA, Zhang Y, Spevak W, Lin J, Phan NY, Habets G, Rymar A, Tsang G, Walters J, Nespi M, Singh P, Broome S, Ibrahim P, Zhang C, Bollag G, West BL, and Green KN. 2019. Sustained microglial depletion with

CSF1R inhibitor impairs parenchymal plaque development in an Alzheimer's disease model. Nat Commun. 10:3758. [PubMed: 31434879]

Sun D, and Jakobs TC. 2012. Structural remodeling of astrocytes in the injured CNS. Neuroscientist. 18:567–588. [PubMed: 21982954]

Sun D, Lye-Barthel M, Masland RH, and Jakobs TC. 2010. Structural remodeling of fibrous astrocytes after axonal injury. J Neurosci. 30:14008–14019. [PubMed: 20962222]

Sun D, Moore S, and Jakobs TC. 2017. Optic nerve astrocyte reactivity protects function in experimental glaucoma and other nerve injuries. J Exp Med. 214:1411–1430. [PubMed: 28416649]

Sun D, Qu J, and Jakobs TC. 2013. Reversible reactivity by optic nerve astrocytes. Glia. 61:1218–1235. [PubMed: 23650091]

Szalay G, Martinecz B, Lenart N, Kornyei Z, Orsolits B, Judak L, Csaszar E, Fekete R, West BL, Katona G, Rozsa B, and Denes A. 2016. Microglia protect against brain injury and their selective elimination dysregulates neuronal network activity after stroke. Nat Commun. 7:11499. [PubMed: 27139776]

Szeto GL, Pomerantz JL, Graham DR, and Clements JE. 2011. Minocycline suppresses activation of nuclear factor of activated T cells 1 (NFAT1) in human CD4+ T cells. J Biol Chem. 286:11275–11282. [PubMed: 21282105]

Tehrani S, Davis L, Cepurna WO, Choe TE, Lozano DC, Monfared A, Cooper L, Cheng J, Johnson EC, and Morrison JC. 2016. Astrocyte Structural and Molecular Response to Elevated Intraocular Pressure Occurs Rapidly and Precedes Axonal Tubulin Rearrangement within the Optic Nerve Head in a Rat Model. PLoS One. 11:e0167364. [PubMed: 27893827]

Tehrani S, Johnson EC, Cepurna WO, and Morrison JC. 2014. Astrocyte processes label for filamentous actin and reorient early within the optic nerve head in a rat glaucoma model. Invest Ophthalmol Vis Sci. 55:6945–6952. [PubMed: 25257054]

Tikka T, Fiebich BL, Goldsteins G, Keinanen R, and Koistinaho J. 2001. Minocycline, a tetracycline derivative, is neuroprotective against excitotoxicity by inhibiting activation and proliferation of microglia. J Neurosci. 21:2580–2588. [PubMed: 11306611]

Tribble JR, Harder JM, Williams PA, and John SWM. 2020. Ocular hypertension suppresses homeostatic gene expression in optic nerve head microglia of DBA/2 J mice. Mol Brain. 13:81. [PubMed: 32450896]

Tribble JR, Kokkali E, Otmani A, Plastino F, Lardner E, Vohra R, Kolko M, Andre H, Morgan JE, and Williams PA. 2021. When Is a Control Not a Control? Reactive Microglia Occur Throughout the Control Contralateral Pathway of Retinal Ganglion Cell Projections in Experimental Glaucoma. Transl Vis Sci Technol. 10:22.

Wang R, Seifert P, and Jakobs TC. 2017. Astrocytes in the Optic Nerve Head of Glaucomatous Mice Display a Characteristic Reactive Phenotype. Invest Ophthalmol Vis Sci. 58:924–932. [PubMed: 28170536]

Wilhelmsson U, Bushong EA, Price DL, Smarr BL, Phung V, Terada M, Ellisman MH, and Pekny M. 2006. Redefining the concept of reactive astrocytes as cells that remain within their unique domains upon reaction to injury. Proc Natl Acad Sci U S A. 103:17513–17518. [PubMed: 17090684]

Xavier AL, Lima FR, Nedergaard M, and Menezes JR. 2015. Ontogeny of CX3CR1-EGFP expressing cells unveil microglia as an integral component of the postnatal subventricular zone. Front Cell Neurosci. 9:37. [PubMed: 25741237]

Yrjanheikki J, Tikka T, Keinanen R, Goldsteins G, Chan PH, and Koistinaho J. 1999. A tetracycline derivative, minocycline, reduces inflammation and protects against focal cerebral ischemia with a wide therapeutic window. Proc Natl Acad Sci U S A. 96:13496–13500. [PubMed: 10557349]

Yuan L, and Neufeld AH. 2001. Activated microglia in the human glaucomatous optic nerve head. J Neurosci Res. 64:523–532. [PubMed: 11391707]

Zamanian JL, Xu L, Foo LC, Nouri N, Zhou L, Giffard RG, and Barres BA. 2012. Genomic analysis of reactive astrogliosis. J Neurosci. 32:6391–6410. [PubMed: 22553043]

Zhao X, Sun R, Luo X, Wang F, and Sun X. 2021. The Interaction Between Microglia and Macroglia in Glaucoma. Front Neurosci. 15:610788. [PubMed: 34121982]

Zhu Y, Pappas AC, Wang R, Seifert P, Sun D, and Jakobs TC. 2018. Ultrastructural Morphology of the Optic Nerve Head in Aged and Glaucomatous Mice. Invest Ophthalmol Vis Sci. 59:3984–3996. [PubMed: 30098187]

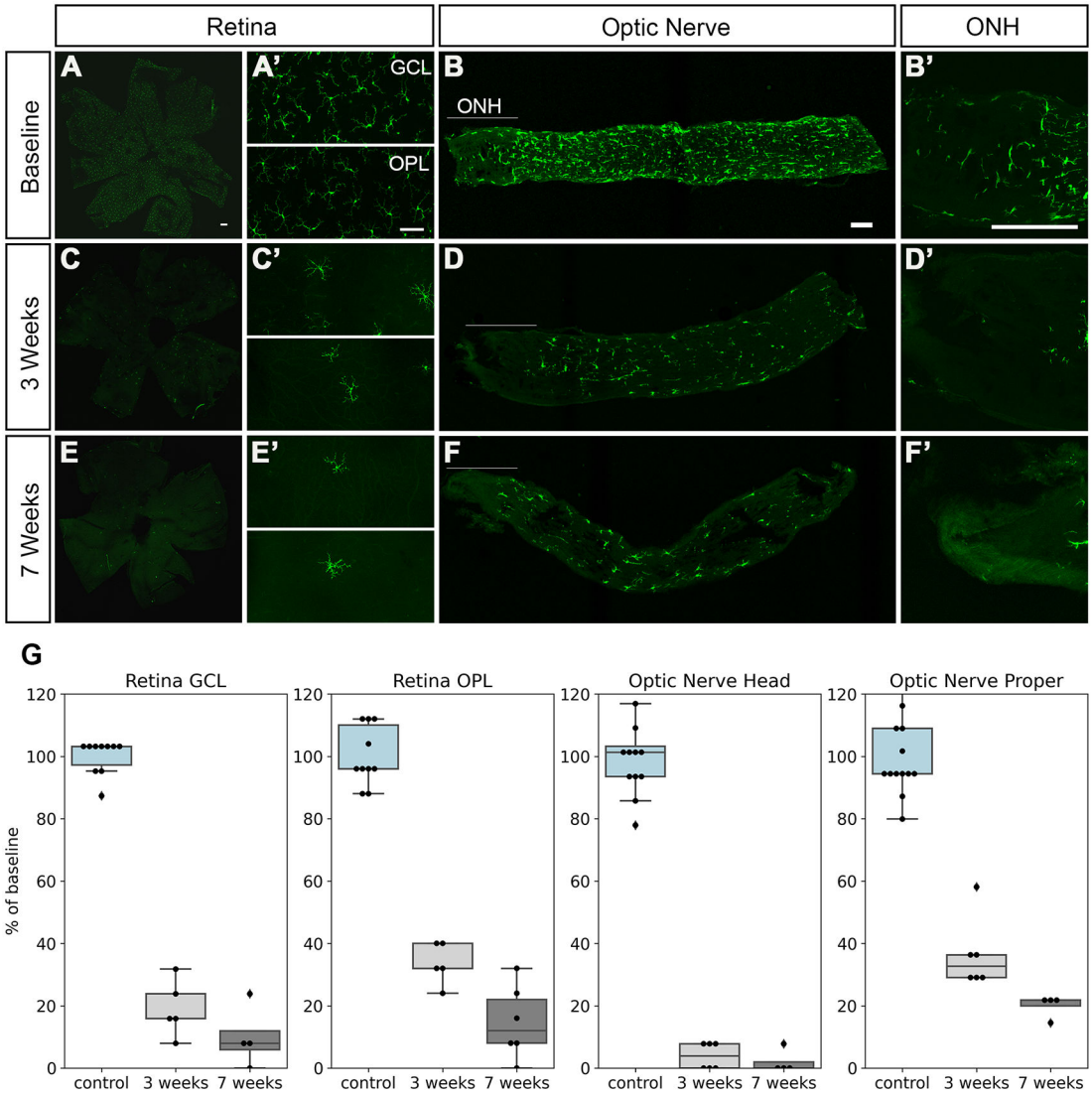

Figure 1.

Microglia depletion by PLX5622. Retinas, optic nerves, and optic nerve heads (ONH) from Cx3cr1-GFP mice were imaged at baseline, 3 weeks, and 7 weeks on the PLX5622 diet. At baseline, GFP^+ cells with the morphology of resting microglia were present throughout the retina (**A, A'**), optic nerve (**B**), and optic nerve head (**B'**). The number of GFP^+ cells decreased markedly at 3 weeks (**C, D**), and even more so at 7 weeks (**E, F**), but some labeled cells persisted, especially in the optic nerve proper (myelinated region of the optic nerve). Scale bars, 50 μm. **G**, quantification of GFP^+ microglial cells. Baseline (control) shown in light blue, 3 weeks light gray, 7 weeks dark gray.

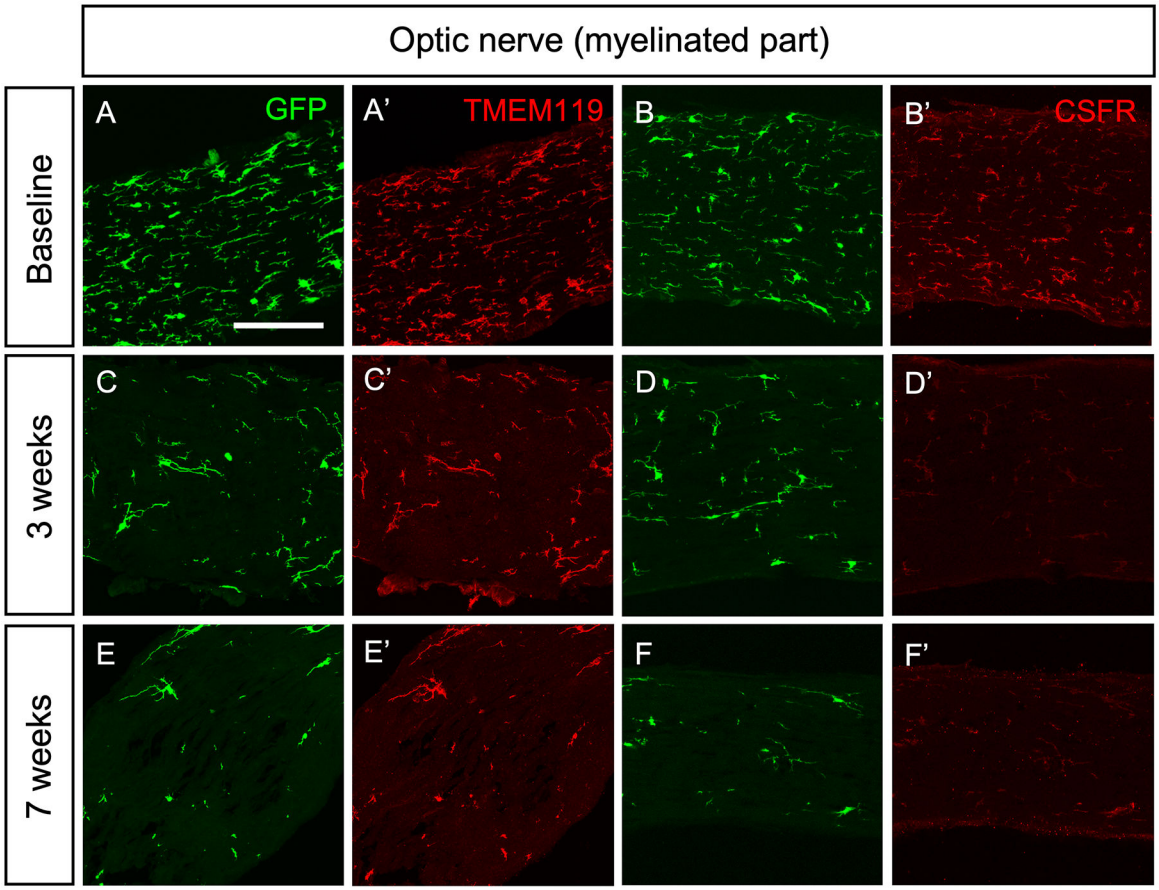

Figure 2.

Counterstaining of GFP+ with microglial markers TMEM119 and CSF1R in the optic nerve proper. All of the GFP^+ cells were co-localized with the microglia marker TMEM119 and the CSF1R. Even after 7 weeks on the PLX5622 diet, some $GFP^+/TMEM119^+$ cells persisted in the optic nerve proper. Scale bars, 50 μm.

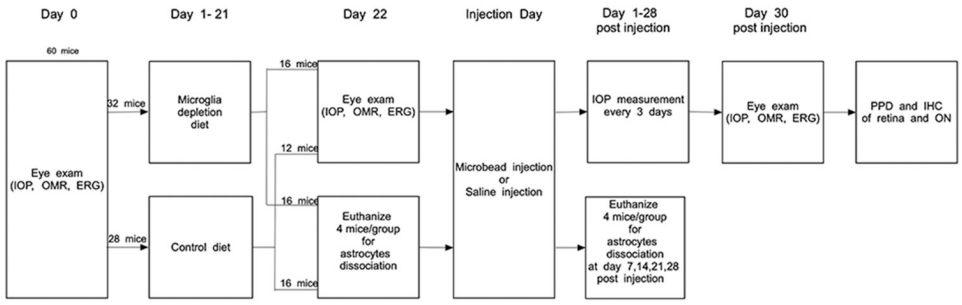

Figure 3.

Experimental design. Age-matched male and female C57bl/6 mice were assigned to experimental groups as shown. Mice in the microglia depletion diet group received PLX5622 in the chow. IOP, intraocular pressure; OMR, optomotor reflex; ERG, pattern electroretinogram.

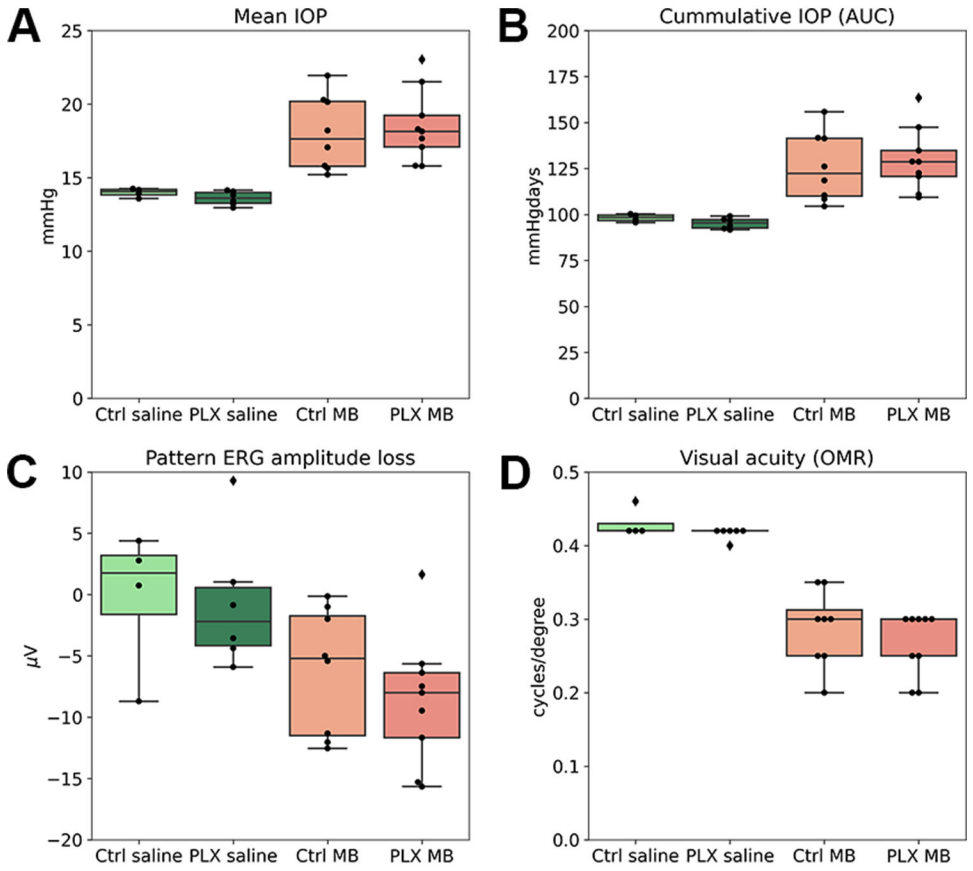

Figure 4.

Induction of elevated IOP by microbead injection. **A-B**, mean IOP in C57bl/6 mice was not affected by PLX5622. Saline-injected mice on the control diet (light green) and the depletion diet (dark green) showed similar mean and cumulative IOPs. Mean and cumulative IOPs were significantly higher in microbead injected mice, both on the control diet (light red) and the PLX5622 diet (dark red). **C**, 4 weeks after microbead injection, the pattern ERG amplitude decreased, but there was no significant difference between mice on the control and the depletion diet. **D**, visual acuity (measured by observation of the oculomotor reflex) decreased in microbead-injected eyes compared to the saline-injected control group, but there was no difference between mice on the control diet and the depletion diet.

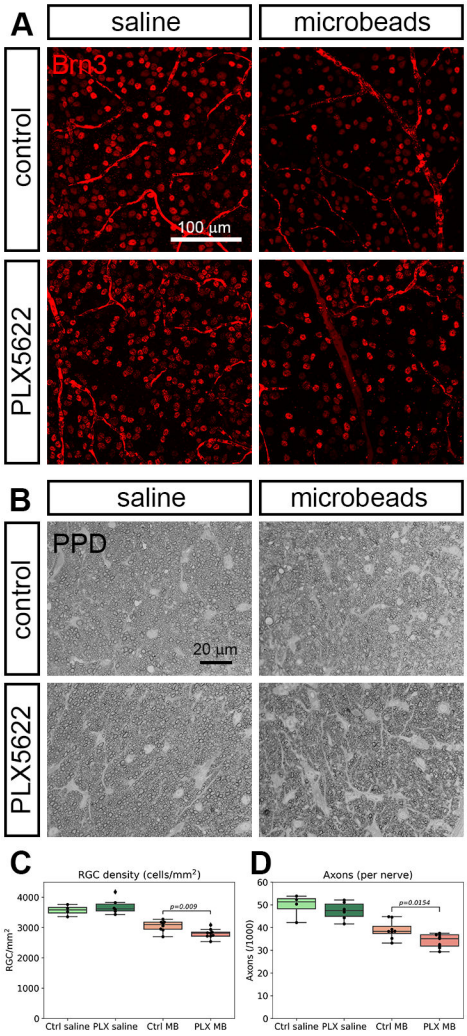

Figure 5.

Retinal ganglion cell and axon counts. **A**, retinal whole-mounts 4 weeks after injection with saline or microbeads were stained with the ganglion cell marker Brn3. Microbead injection leads to a loss of retinal ganglion cells that is more severe if the mice had received the microglia depletion diet. **B**, ganglion cell axons were stained with p-phenylenediamine (PPD) and counted. **C**, quantification of retinal ganglion cell density in the four experimental groups (regular diet and saline injection, light green; PLX5622 diet and saline injection, dark green; regular diet and microbead injection, light red; PLX5622 diet and microbead injection, dark red). **D**, quantification of the axon counts. Color code as in C.

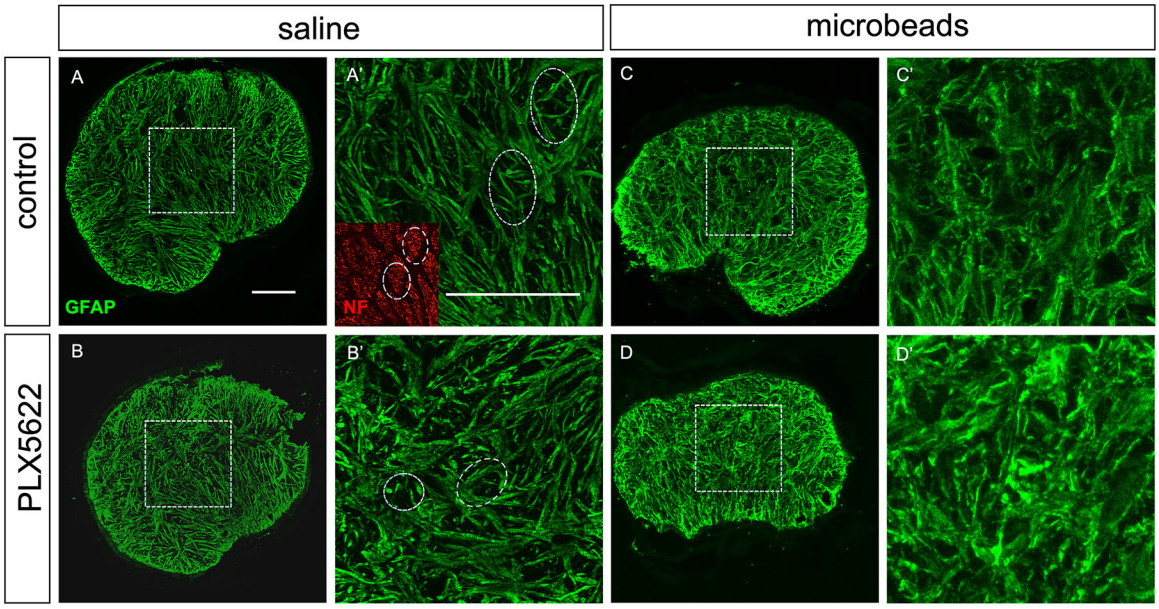

Figure 6.

Astrocyte morphology. **A-B**, transverse sections of optic nerve heads (unmyelinated region) of saline-injected eyes stained with anti-GFAP antibodies. Microglia depletion by itself did not change astrocyte morphology. **A'** and **B'** show higher-magnification views of the boxed areas in A and B. Glial tubes through which ganglion cell axon bundles pass are indicated with white ovals. The inset in **A'** shows axons stained with an antibody to neurofilament heavy chain (NF). **C-D**, astrocytes after microbead injection show the typical morphological signs of reactivity (process thickening and loss of glial tubes), but there was no difference between the control and the microglia-depleted groups. **E**, astrocyte process thickness was measured in optic nerves from 4 mice per group.

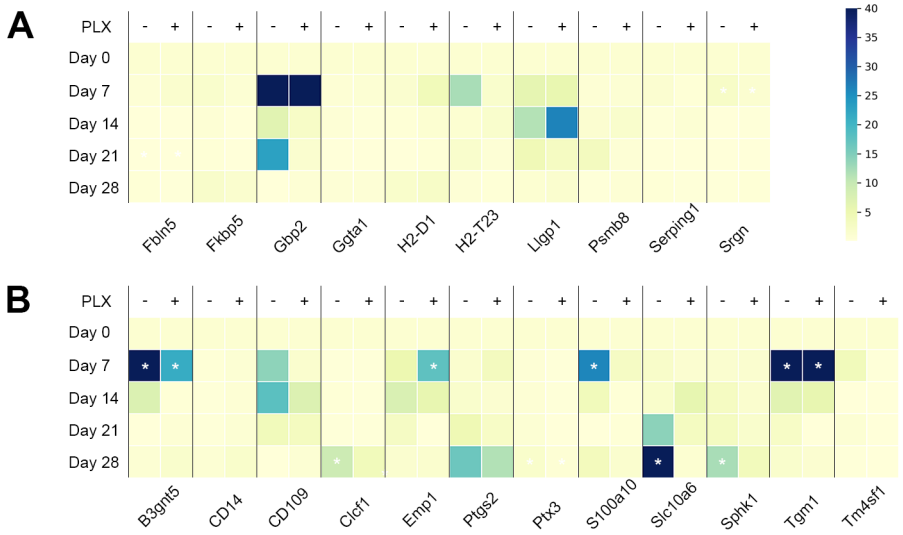

Figure 7.

Time series of A1 and A2 genes in optic nerve head astrocytes. **A**, genes in the “A1”, or neurotoxic group. Gpb2 was at the level of detection at day 0, but became detectable thereafter. **B**, genes in the “A2”, or neuroprotective group. Color bar for panels A-B, colors represent –fold expression compared to baseline (Day 0). White asterisks indicate significant differences from the baseline expression levels.